ORIGINAL PAPER

Synthesis and characterization of electrospun composite nanofibers from *Moringa oleifera* biomass and metal oxide nanoparticles as potential adsorbents for the removal of lead ions

Ronald Ngulube[1] · Letitia Pillay[2] · Nolwazi Nombona[1]

Abstract

Electrospun multicomposite nanofibers synthesized from extracts of *Moringa oleifera* (*M. oleifera*) seed biomass blended with metal oxide nanoparticles (MONPs) and polyacrylonitrile (PAN) were investigated as potential adsorbents. The materials were characterized using SEM, XRD, FTIR, BET and TGA. The specific surface area of MONPs ranged between 29.75 and 60.92 m^2/g and their incorporation in the PAN/*M. oleifera* composite blend resulted in increased surface coarseness and larger nanofiber diameters (268 ± 21–317 ± 27 nm). The application of PAN/*M. oleifera*/MONPs for Pb(II) removal from aqueous solution via batch adsorption experiments was investigated based on the parameters: solution pH, contact time and initial Pb(II) ion concentration. Experimental results better fitted the Langmuir isotherm model and pseudo-second-order kinetics. Adsorption capacities ranged between 172.4 and 227.3 mg/g. These results demonstrate that low-cost indigenous materials have significance and applicability in water remediation applications.

Keywords Electrospinning · Nanofiber · *Moringa oleifera* · Lead ions · Adsorption

Introduction

In most parts of the world, a large number of people rely on ground or surface water for sustenance. However, mining, industrial and agricultural activities have led to contamination of these water sources. Organic matter and heavy metals are the most significant pollutants (Ghomi et al. 2020; Ibrahim et al. 2021; Pereao et al. 2017; Sakib et al. 2021). Heavy metal ions are the most widely known toxic pollutants, as they are ubiquitous and non-degradable in the environment. They can be mobile, absorbed by living organisms and toxic even at low concentrations (Babel and Kurniawan 2004; Liu et al. 2022; Martín et al. 2018; Morillo et al. 2017). Human exposure to elevated concentrations of toxic metals (e.g., Pb, Cd, Hg, As, Cr) from the environment may cause severe health issues, including neurological damage, liver, or kidney dysfunction and cancer (Khalid et al. 2021; Khlifi and Hamza-Chaffai 2010; Moonga et al. 2022). This makes access to clean potable water one of the largest challenges facing many countries and, in particular, third world countries.

Remediation approaches developed and utilized thus far attempt to remove metals from water by precipitation (Fu and Wang 2011), electroplating (Yong et al. 2021), coagulation (Zheng et al. 2021), membrane separation (Tempelman et al. 2019), ion exchange (Dąbrowski et al. 2004) and adsorption (Galiano et al. 2018). Adsorption is widely studied as it translates to technologies that are simple, economical and effective (Crini et al. 2018). However, most of the conventional adsorbents (clay, activated carbon, wood sawdust) used have limitations such as low adsorption capacities, lack of functional tunability and reusability (Sarode et al. 2019). These challenges have given rise to the search for new sorbent materials.

The use of nanofibers has stimulated increased research interest in water remediation via adsorption technology. Moreover, electrospinning has been recognized as the most promising technique for fabricating nanofibers, as it provides flexibility to regulate morphology, size, surface area and porosity (Deitzel et al. 2002; Pereao et al. 2017). New

✉ Nolwazi Nombona
nolwazi.nombona@up.ac.za

1 Department of Chemistry, University of Pretoria, Pretoria 0002, South Africa

2 Molecular Sciences Institute, University of the Witwatersrand, Johannesburg 2000, South Africa

trends in developing nanofibers from natural polymers such as cellulose, alginates, chitosan, hyaluronic acid, keratin and silk fibroin have attracted attention because of their renewability, biodegradability, nontoxicity, biocompatibility and availability (Cui et al. 2020; Deng et al. 2021; Jain et al. 2020; Khademian et al. 2020; Raza et al. 2021; Wen et al. 2017). The presence of functional groups (e.g., hydroxyl, carboxyl and amine) in the chemical structure enables these biopolymers to have a strong coordinative affinity in forming chelate complexes with several heavy metal ions (Khademian et al. 2020; Kyzas et al. 2009). Despite these attractive attributes, the use of pure biopolymers in the fabrication of nanofibers by electrospinning is still a challenge because they tend to form gels in aqueous media because of hydrogen bonding (Wongkanya et al. 2017). Additionally, they are naturally prone to degradation, resulting in nanofiber structure alteration or damage during application (Wen et al. 2017). Adding biopolymers to the synthetic polymer matrix may alleviate such shortcomings. Several synthetic polymers, e.g., poly(lactide-*co*-glycolide) (PLGA) (Duan et al. 2006), polyvinyl pyrrolidone (PVP) (Ignatova et al. 2007), poly(ethylene terephthalate) (PET) (Jung et al. 2007) and poly(lactic acid) (PLA) (Xu et al. 2009), have been electrospun with biopolymers. The obtained nanofibers showed that the synthetic polymers enhanced the electrospinnability of the biopolymers and resulted in improved mechanical strength and biocompatibility.

Advances in enhancing the adsorption capacity of nanofiber adsorbents have led to the immobilization of metal oxide nanoparticles (MONPs) such as manganese oxide, iron oxide, zinc oxide and titanium oxide into the polymer blend (Deliyanni et al. 2003; Kumar et al. 2013; Li et al. 2018). These MONPs have been reported to impart increased mechanical strength, chemical resistivity, and adsorption capacity of the nanofibers due to their physical and chemical properties (Razzaz et al. 2016). Furthermore, doping MONPs is known to enhance nanoparticles (NPs) affinity toward particular analytes such as heavy metals because of change in the surface reactivity (Chakrabarti et al. 2005; Ghiloufi et al. 2016; Montoya et al. 2017; Warner et al. 2012). This has the effect of tailoring the selectivity of MONPs toward heavy metal ions of interest. However, the properties of the nanocomposite sorbents depend, to a large extent, on how well the NPs are dispersed within the biopolymer matrix, their interaction and bonding structure (An et al. 2009; Liu et al. 2015; Sarkar et al. 2012). Therefore, an optimal balance between material strength and adsorption efficiency should be maintained to prevent inaccessibility of active adsorption sites.

Keshtkar et al. (2016) investigated the adsorption of Cd(II), Pb(II) and Ni(II) ions from aqueous solution using an electrospun polyvinylpyrrolidone/silica/3-aminopropyltriethoxysilane (PVP/SiO$_2$/APTES) composite nanofiber adsorbent. The maximum adsorption capacities for Cd(II), Pb(II) and Ni(II) ions were found to be 157.4, 158.3 and 63.0 mg/g, respectively. These values were related to the large surface area together with the inter- and intrafibrous pores of the composite nanofiber adsorbent resulting in increased adsorption capacity. Bahmani et al. (2019) used a composite nanofiber consisting of polyacrylonitrile (PAN) and Fe$_2$O$_3$ NPs for As(V) ion removal from aqueous solution. The maximum adsorption capacity achieved with 0.5 wt% Fe$_2$O$_3$ NPs was 71.9 mg/g compared to 82.2 mg/g recorded for 1.0 wt% Fe$_2$O$_3$ NPs. The enhanced adsorption capacity observed for the 1.0 wt% Fe$_2$O$_3$ NPs composite material was due to the availability of more chelating groups from the Fe$_2$O$_3$ NPs, to bind As(V) ions. Parlayıcı et al. (2016) synthesized an electrospun PAN/TiO$_2$ nanofiber at 1.0 and 3.0 wt% amounts of TiO$_2$ NPs. The nanofibers achieved adsorption capacities for Cr(VI) ions of 245.3 and 280.4 mg/g for 1.0 and 3.0 wt% PAN/TiO$_2$ nanofibers, respectively. The adsorption mechanism was enhanced due to electrostatic attraction, surface complexation and coordination. Vázquez-Guerrero et al. (2021) incorporated Fe$_2$O$_3$ NPs into cellulose nanofibers to improve Cd (II) and Pb(II) ion adsorption and maximum adsorption capacities of 12 and 81 mg/g were achieved, respectively. The results showed that the impregnation of Fe$_2$O$_3$ within the nanofibers enhanced the adsorption performance for the uptake of metal ions in aqueous solution.

We report the combined use of *M. oleifera*, MONPs and PAN in the development of nanocomposite adsorbents through the electrospinning process. There are currently several reports on the use of *M. oleifera* as a natural coagulant for water purification. The plant extract contains dimeric cationic proteins with the resultant surface charge increasing its capacity for adsorption (Ali 2016; Ndabigengesere and Narasiah 1998; Okuda et al. 2001). Its use incorporated with metal oxides into nanofibers for adsorption applications is limited.

Experimental

Materials

Iron(III) chloride (FeCl$_3$, 99%), iron(II) sulfate heptahydrate (FeSO$_4$·7H$_2$O), manganese(II) sulfate (MnSO$_4$. H$_2$O), cobalt(II) sulfate (CoSO$_4$), potassium permanganate (KMnO$_4$), sodium hydroxide (NaOH), hydrochloric acid (HCl), polyacrylonitrile (PAN) average MW 150000, *N*, *N*-dimethylformamide (DMF), sodium chloride (NaCl), lead nitrate (PbNO$_3$, 98%) and ethanol were of analytical grade and used as purchased from Sigma-Aldrich. *M. oleifera* seeds were purchased from Umoyo Natural Health Store, Zambia.

Instrumentation

The blended polymer solutions were electrospun using an electrospinning unit. The voltage was supplied by a high-voltage power supply (JDF-1, Beijing, China), and the feeding rate of the solution was controlled by a syringe driver (789100C, Cole-Parmer, Vernon Hills, IL, USA). The nanofiber mats were collected on aluminum foil fitted to the collector, which was placed vertically to the needle tip.

The surface morphology of the materials was examined using a Zeiss Crossbeam 540 field emission-scanning electron microscope (FE-SEM) operated at 2.00 kV. The crossbeam 540 FEG was coupled with energy-dispersive X-ray spectroscopy, which was used to determine the elemental composition of the samples. To prevent electrostatic charging during analysis, the material samples were coated with a thin layer of carbon. ImageJ software was used to estimate the average NPs and fiber diameters. N_2 absorption/desorption isotherms were obtained on a Micromeritics TriStar II 3020 Analyzer at -196 °C, operated in a relative pressure (P/Po) range of 0–1.0 with pre-degassing of the samples at 100 °C for 18 h under vacuum prior to the measurement. The Brunauer–Emmett–Teller (BET) and Barrett–Joyner–Halenda (BJH) models were used to determine the surface area, pore volume and size of the samples. X-ray diffraction (XRD) patterns were obtained using a Bruker D2 Phaser X-ray diffractometer (XRD) with CuK$_\alpha$ radiation, a 0.15418 nm wavelength and a scanning speed of 0.05° per minute. Infrared (IR) spectra were recorded using an Alpha (II) Brucker spectrometer.

Synthesis of NPs

Fe3O4 NPs

Fe_3O_4 NPs were synthesized by chemical co-precipitation of Fe^{3+} and Fe^{2+} with NaOH (Mascolo et al. 2013). In a typical experiment, 0.02 mol of $FeCl_3$ and 0.01 mol of $FeSO_4 \cdot 7H_2O$ were dissolved in 100 mL degassed, deionized water and the mixture was sonicated for 15 min. A precipitating agent was prepared by dissolving 0.08 mol of NaOH in 100 mL degassed, deionized water which was added dropwise into the reaction mixture at room temperature (25 °C) under nitrogen gas while stirring. The mixture was stirred for 3 h, and the obtained precipitate was washed with deionized water and rinsed several times with ethanol. The particles were separated from the supernatant by centrifugation and were dried under vacuum at 80 °C for 6 h.

Co-doped Fe$_3$O$_4$ NPs

Synthesis of Co-doped Fe_3O_4 NPs was carried out based on a modified co-precipitation method (Wahab et al. 2019).

In brief, 0.014 mol of $FeCl_3$ and 0.007 mol of $FeSO_4 \cdot 7H_2O$ were dissolved in 50 mL of degassed, deionized water at room temperature. The mixture was sonicated for 15 min followed by the addition of $CoSO_4$ (0.04 M, 10 mL), and the mixture was stirred for 10 min. Thereafter, NaOH (0.25 M, 40 mL) in degassed water was added to the reaction mixture dropwise. The mixture was placed in a Teflon-lined stainless-steel autoclave and heated at 160 °C for 4 h. The mixture was cooled, and the particles were washed with deionized water, rinsed with ethanol and dried under vacuum for 6 h at 80 °C.

Mn-doped Fe3O4 NPs

Synthesis of Mn-doped Fe_3O_4 NPs was adapted from Warner et al. (2012) with minor modification. Briefly, 1.0 g of Fe_3O_4 NPs was suspended in 50 mL degassed, deionized water and sonicated for 30 min. To this mixture, $MnSO_4$ (0.009 M, 10 mL) in water was added and stirred for 50 min, followed by the addition of $KMnO_4$ (0.009 M, 10 mL) in water. The reaction mixture was stirred for 1 h at room temperature, and the formed particles were separated, washed, and rinsed with ethanol to remove traces of $KMnO_4$. The particles were dried in an oven at 120 °C for 2 h.

Co- and Mn-doped Fe3O4 NPs

Co- and Mn-doped Fe_3O_4 NPs were prepared following the method reported for Co-doped Fe_3O_4 NPs. However, $CoSO_4$ (0.02 M, 10 mL) and $MnSO_4$ (0.02 M, 10 mL) were added prior to the dropwise addition of NaOH.

M. oleifera biomass solution preparation

Finely ground *M. oleifera* seed powder was added to a 95% ethanol aqueous solution and stirred for 30 min to defat the powder. The powder was separated by centrifugation and dried at room temperature for 24 h (dos Santos et al. 2016). The *M. oleifera* extract was obtained by adding 1.0 g of defatted powder to aqueous NaCl (1 M, 100 mL) solution. The solution was stirred for 1 h, and the extract was separated by filtration. The filtrate was frozen at -4 °C for 24 h and then freeze-dried. The obtained white powder was stored at room temperature.

Synthesis of nanofibers

PAN/M. oleifera nanofibers

The PAN/*M. oleifera* mats were fabricated using the electrospinning technique. Briefly, 8% (w/v) PAN solution was prepared by dissolving 0.8 g of PAN polymer powder in 10 mL DMF solution. The mixture was stirred for 8 h to

form a homogeneous solution. Then 3.0 g *M. oleifera* powder was added to the homogeneous solution, and stirring was continued for another 5 h to facilitate complete dissolution. The blended suspension was electrospun under optimal conditions (flow rate of 0.8 mL/h, applied voltage of 10 kV, and tip-to-collector distance of 15 cm). The nanofibrous mats obtained were placed in a vacuum oven (160 °C, 60 min) to increase their stability in water. The mats were detached from the aluminum foil and cut into 2 cm×2 cm sections.

PAN/M. oleifera/MONPs nanofibers

PAN/*M. oleifera*/MONPs mats were prepared by adding 0.8 g of PAN to 10 mL of DMF solution. The mixture was stirred for 8 h to form a homogeneous solution. To this, 1.5 g *M. oleifera* powder and 1.0 g MONPs powder were simultaneously added, and stirring was continued for another 5 h. The solution was sonicated for 5 min prior electrospinning. The solution was electrospun using the optimal conditions listed in the previous section.

Surface charge characterization of nanofiber mats

The initial pH of the analyte solution plays a significant role in the adsorption process, as it influences the degree of ionization/dissociation of surface functional groups on the adsorbent. This can be explained by the adsorbent point of zero charge (pH_{pzc}), defined as the pH at which the surface charge density of the material is zero. Surface charge characterization of the fabricated nanofibers was determined by the solid addition method (Naiya et al. 2009). Nanofiber mats were cut into 5 mg pieces and placed in 0.01 M NaCl solutions with varying pH values (2.5–9.0). The solution was stirred for 48 h, and the pH was measured thereafter. The pH_{pzc} was determined by plotting the difference in initial pH (pH_0) and final pH (pH_f) values against pH_0. The point of intersection of the resulting curve with pH_0 gives the point of zero charge (Zhao et al. 2015).

Adsorption experiments

Batch adsorption experiments were performed to investigate the adsorption behavior of electrospun composite nanofibers at different parameters such as solution pH, contact time and initial Pb(II) concentration. In order to achieve this, the composite nanofiber mat of mass 1.0 mg was immersed in 20 mL of Pb(II) solution (5 mg/L) while shaken at 100 rpm under ambient conditions. The initial pH of the Pb(II) solution was varied in the range of 3–10. The effect of contact time and initial Pb(II) concentration was studied in the range of 30–150 min and 1–30 mg/L, respectively. The concentrations of the metal ions were determined using ICP-MS. The equilibrium adsorption capacity (q_e) was calculated using Eq. (1) (Chang et al.

2016); Tan et al. 2016). Blank experiments were conducted to validate the adsorption experiments. All the adsorption experiments were carried out in triplicate for statistical purposes, and the averaged values were reported.

$$q_e = \frac{(C_i - C_e) \times V}{m} \tag{1}$$

where C_i and C_e are the initial and equilibrium concentration, respectively (mg/L), V is the volume of the solution (L) and m is the mass of fiber mat used (g).

Adsorption isotherms

Adsorption isotherms are essential in understanding the adsorption process and represent the interaction between the amounts of the adsorbate adsorbed on the surface of the adsorbent at equilibrium concentration (Bharathi and Ramesh 2013). The Langmuir and Freundlich isotherms are the most widely used models as they give information pertaining to the maximum adsorption capacity and binding mechanisms. With respect to the Langmuir isotherm, it is assumed that the adsorbent has a homogenous surface and can only allow monolayer adsorption. This model can be described by Eq. (2) (Fan et al. 2012).

$$\frac{C_e}{q_e} = \frac{C_e}{q_m} + \frac{1}{K_L q_m} \tag{2}$$

where q_m is the maximum amount of adsorption (mg/g) and K_L is the Langmuir constant related to binding energy between the adsorbate and adsorbent (L/mg).

K_L can be used to determine the separation factor, R_L. The R_L value gives information on the strength of adsorption and is defined by Eq. (3) (Hasan et al. 2012).

$$R_L = \frac{1}{1 + K_L C_i} \tag{3}$$

The Freundlich isotherm on the other hand assumes multilayer and heterogeneous adsorption of solute on an adsorbent surface and is expressed by Eq. (4) (Li et al. 2003).

$$\log q_e = \log K_F + \frac{1}{n} \log C_e \tag{4}$$

where K_F is the Freundlich constant and is related to the binding capacity between absorbent and adsorbate and n represents the empirical constant that indicates heterogeneity factor and is related to the sorption intensity.

Adsorption kinetics

Adsorption kinetic models are formulated on the assumption of the surface reaction being the limiting step in the

adsorption process without consideration of the diffusive transfer of metal ions onto the adsorbent (Nurlilasari et al. 2019). The adsorption kinetics were investigated using pseudo-first-order and pseudo-second-order kinetic studies. The pseudo-first-order model assumes physical adsorption as the dominant mechanism. It can be represented according to Eq. (5) (Wang et al. 2014).

$$\log (q_e - q_t) = \log \left(q_e \right) - k_1 \tag{5}$$

where k_1 is the pseudo-first-order rate constant (min^{-1})

While the pseudo-second-order model indicates chemisorption as the rate-limiting step (Cai et al. 2017), the pseudo-second-order model can be expressed using Eq. (6).

$$\frac{t}{q_t} = \left(\frac{1}{q_e} \right) t + \left(\frac{1}{k_2 q_e^2} \right) \tag{6}$$

where k_2 is the pseudo-second-order rate constant (g/mg.min)

Results and discussion

SEM micrographs of the synthesized material

MONPs

SEM images show the morphology of the synthesized MONPs as presented in Fig. 1. The Fe_3O_4 particles were predominantly spherical and agglomerated. The metal-doped Fe_3O_4 particles exhibited an identical shape as the prepared Fe_3O_4 particles, suggesting that the surface morphology was nearly unchanged during the co-precipitation process (Nurlilasari et al. 2019). According to Atacan et al. (2018), MONPs tend to agglomerate to reduce the high surface energy they possess. SEM images also reveal that the mean diameters of the MONPs are different, ranging between 46 ± 5 and 58 ± 6 nm as can be seen in Fig. S1 in the Supplementary Information, suggesting that the Fe^{3+} and Fe^{2+} ions of Fe_3O_4 are substituted by metal dopants (Co^{2+} and Mn^{2+}) of different radii (Suresh et al. 2012). SEM–EDX

analysis shown in Fig. S2 further confirmed the successful synthesis of the NPs. Fig. S2a shows the presence of iron and oxygen in Fe_3O_4, and Fig. S2b–d shows the presence of cobalt, manganese or both for the correspondingly doped Fe_3O_4.

Table 1 shows the specific surface areas, pore volumes and pore diameters obtained for the MONPs. Analysis of the Fe_3O_4 NPs before and after doping with Co^{2+} showed an increase in the specific surface area from 61 to 65 m^2/g. Similarly, an increase in the specific surface area to 80 m^2/g was observed when Mn^{2+} dopant was added to the Fe_3O_4 structure. The large specific surface area confirms a high number of active sites available for adsorption on the surface of the nanoparticles. When dopants with different atomic sizes compared to the parent crystal are added, more imperfections are expected to occur (Wahab et al. 2019; Warner et al. 2012). As previously stated, the Co^{2+} ion has a smaller atomic radius and the Mn^{2+} ion has a larger atomic radius than the parent ions of the ferrite crystal. This implies that the imperfections caused by doping with these metals will cause surface roughness and disorder of the Fe_3O_4 structure leading to increased specific surface area. The inclusion of both Co^{2+} and Mn^{2+} dopants in the Fe_3O_4 mother structure resulted in a significantly decreased specific surface area of 30 m^2/g and the lowest pore volume of 0.08 cm^3/g (Table 1). This reduction may be related to the observed agglomeration of the Fe_3O_4:Co-Mn NPs as observed in SEM images. Even though agglomeration is observed in all NPs, the large particle size of Fe_3O_4:Co-Mn NPs may also contribute toward reducing the specific surface area. Increased agglomeration

Table 1 Textual properties of the MONPs

Sample	Specific surface area (m^2/g)	Pore volume (cm^3/g)	Pore diameter (nm)
Fe_3O_4 NPs	61	0.21	3.73
Fe_3O_4:Co NPs	65	0.22	3.90
Fe_3O_4:Mn NPs	80	0.25	3.90
Fe_3O_4:Co-Mn NPs	30	0.08	2.72
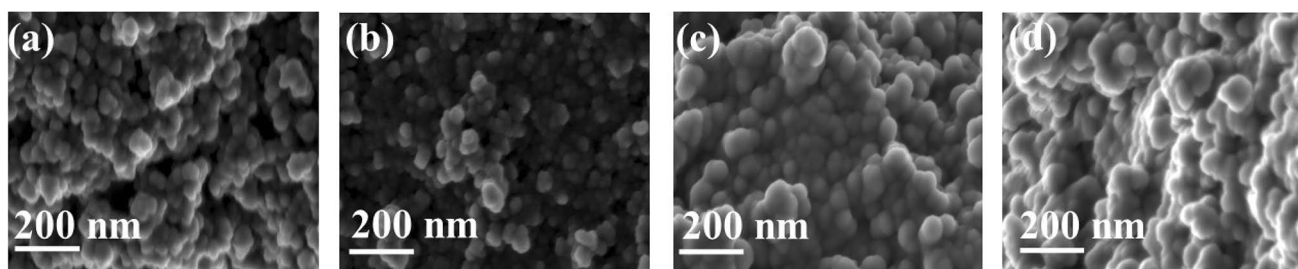
Fig. 1 SEM images of **a** Fe_3O_4, **b** Fe_3O_4:Co, **c** Fe_3O_4:Mn and **d** Fe_3O_4:Co-Mn NPs

of particles has been found to reduce the specific surface area of doped nanomaterials (Mbakaan et al. 2021). The pore diameters of the materials ranged from 2.72 to 3.90 nm, revealing them as mesoporous. This means that the synthesized nanofiber mats have the capacity to adsorb metal ions.

PAN/M. oleifera and PAN/M. oleifera/MONP nanofibers

SEM images of PAN/*M. oleifera* and PAN/*M.* oleifera/ MONP electrospun fibers have a characteristic interwoven network structure (Fig. S3) caused by thermal cross-linking. The interwoven network structure has been reported to enhance the mechanical strength of fibers (Chen et al. 2019). The fibers are continuous and bead-free as shown in Fig. S3. The PAN/*M. oleifera* fibers (Fig. 2a) exhibited an uneven outer surface with an average diameter of 218 ± 22 nm (Fig. S4a). Incorporation of MONPs in the PAN/*M. oleifera* blend resulted in surface roughness of the fibers (Fig. 2b–e) and an increased mean diameter (268 ± 21–317 ± 27 nm) (Fig. S4b–e). The surface roughness may be an indication that the MONPs are incorporated inside the nanofibers. The enhanced surface roughness is expected to increase the surface area of the composite nanofibers. The increased fiber diameter upon the addition of MONPs was attributed to the higher viscosity of the polymer composite (Lee et al. 2018; Liu et al. 2015; Ramakrishna et al. 2006).

FTIR analysis

FTIR spectroscopy was used to identify specific functional groups in the synthesized nanofibers (Fig. 3). This is essential for gaining insight into the adsorption mechanism of the fibers. Functional groups identified in Fig. 3a include a broad peak at 3293 cm^{-1} attributed to O − H stretching within the fatty acids, carbohydrates and protein structure present in the *M. oleifera* seed sample. The peak observed at 2937 cm^{-1} is attributed to C–H stretching, and peaks at 1650 cm^{-1} and 1070 cm^{-1} are attributed to C=O and C–O stretching, respectively (Araújo et al. 2010; Bhutada et al. 2016; Ibrahim et al. 2022; Narayan et al. 2022). The pure PAN (Fig. 3(b)) displayed the characteristic nitrile (C≡N) stretching peak at 2240 cm^{-1} and the alky bond
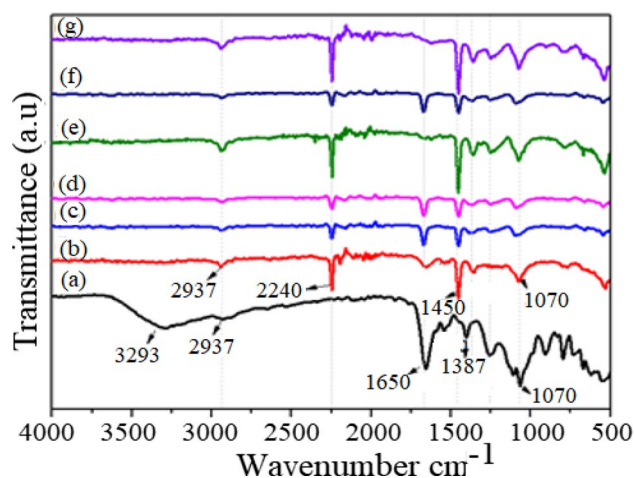

Fig. 3 FTIR spectra of **a** *M. oleifera* powder, **b** PAN powder, **c** PAN/*M. oleifera*, **d** PAN/*M. oleifera*/Fe$_3$O$_4$, **e** PAN/*M. oleifera*/F*e$_3$O$_4$*:Mn, **f** PAN/*M. oleifera*/Fe$_3$O$_4$:Co and **g** PAN/*M. oleifera*/Fe$_3$O$_4$:Co-Mn nanofibers

(C–H) stretching peak at 1450 cm^{-1} (Fayemi et al. 2018; Narayan et al. 2022). The synthesized composite nanofibers (Fig. 3c–g) showed peaks for nitrile stretching at 2240 cm^{-1} from the PAN component, a weak C–H stretching peak at 2937 cm^{-1} from the *M. oleifera* extract with the C=O and C−O peaks at 1650 cm^{-1} and 1070 cm^{-1}, respectively. The results support the suggestion made previously that the *M. oleifera* seed extract and PAN are incorporated within the nanofiber matrix.

X-ray diffraction analysis

The crystal structures of the synthesized MONPs were elucidated by XRD as illustrated in Fig. 4. The positions and relative intensities of the major diffraction peaks of the iron oxide sample were in accordance with the standard Fe$_3$O$_4$ (JCPDS card no. 89–3854) and comparable to other studies (Guo et al. 2011; Klencsár et al. 2019). The major peaks observed at $2\theta = 29.6°$, $34.9°$, $42.6°$, $53.1°$, $56.6°$ and $62.3°$ correspond to the (220), (311), (400), (422), (511) and (440) planes, respectively (Nunes et al. 2006). The presence of
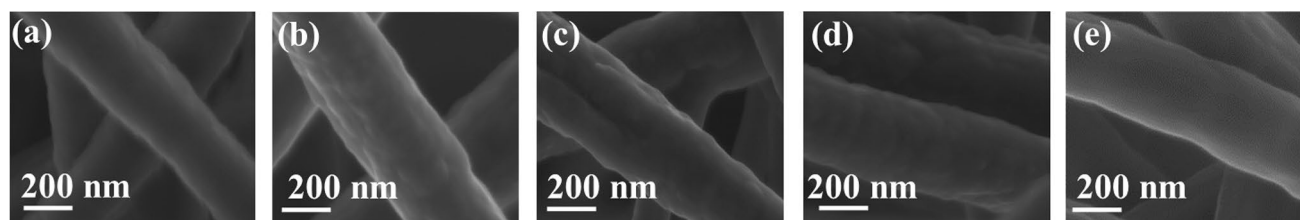

Fig. 2 SEM images of **a** PAN/*M. oleifera*, **b** PAN/*M. oleifera*/Fe$_3$O$_4$, **c** PAN/*M. oleifera*/Fe$_3$O$_4$:Co, **d** PAN/M. *oleifera*/Fe$_3$O$_4$:Mn and **e** PAN/*M. oleifera*/Fe$_3$O$_4$:Co-Mn nanofibers
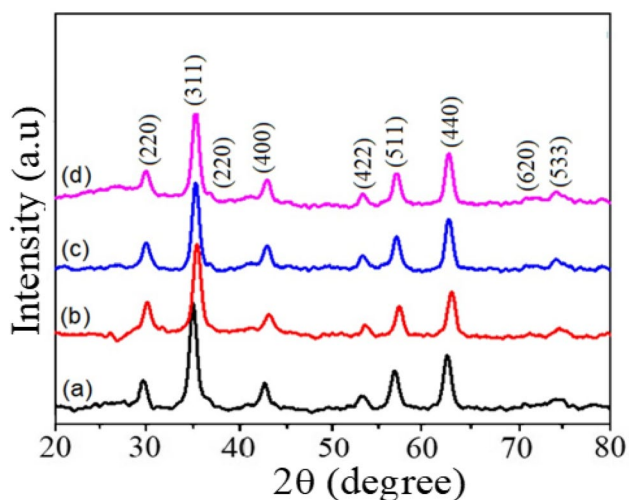
Fig. 4 XRD patterns of **a** Fe$_3$O$_4$, **b** Fe$_3$O$_4$:Co, **c** Fe$_3$O$_4$:Mn and **d** Fe$_3$O$_4$:Co-Mn NPs

confirming the incorporation of Mn^{2+} atoms in the ferrite lattice structure. The Co–Mn-doped Fe$_3$O$_4$ XRD pattern shown in Fig. 4d follows the same pattern as that for Fig. 4c with no shifts or new peaks observed. This confirms that there are no cobalt oxide or manganese oxide peaks and since EDX analysis confirmed the presence of both Co and Mn atoms, and there was a significant change in the specific surface area on the material, doping can be confirmed.

Effect of solution pH

Figure 5a shows the pH$_{pzc}$ of the composite fibers. The pH$_{pzc}$ of PAN/*M. oleifera* nanofiber mat was found to be 6.1. Inclusion of MONPs into PAN/*M. oleifera* blend reduced the pH$_{pzc}$ values to 4.9 (PAN/*M. oleifera*/Fe$_3$O$_4$), 4.8 (PAN/*M. oleifera*/Fe$_3$O$_4$:Mn), and 5.0 (PAN/*M. oleifera*/Fe$_3$O$_4$:Co and PAN/*M. oleifera*/Fe$_3$O$_4$:Co-Mn). The reduced pH$_{pzc}$ indicates that the introduction of MONPs into PAN/*M. oleifera* blend resulted in an increased ionic strength of the fiber mats.

The effect of solution pH on the adsorption of Pb(II) ions onto composite fiber mats was investigated in the range of 3 – 10 while maintaining the initial Pb(II) ions concentration at 5 mg/L. Figure 5b shows the effect of pH on the adsorption capacity of the composite fibers. The PAN/*M. oleifera*/Fe$_3$O$_4$:Mn composite fiber showed the highest adsorption capacity at a wider pH range from 7.5 to 9. At solution pH below the pH$_{PZC}$, the adsorption capacities of the adsorbents are below 58 mg/g. When the solution pH is less than pH$_{PZC}$, the surface of the composite fibers becomes positively charged. As a result of this, adsorption of positively charged Pb(II) ions is least favored due to electrostatic repulsion. This explains the trend observed in Fig. 5b. The results
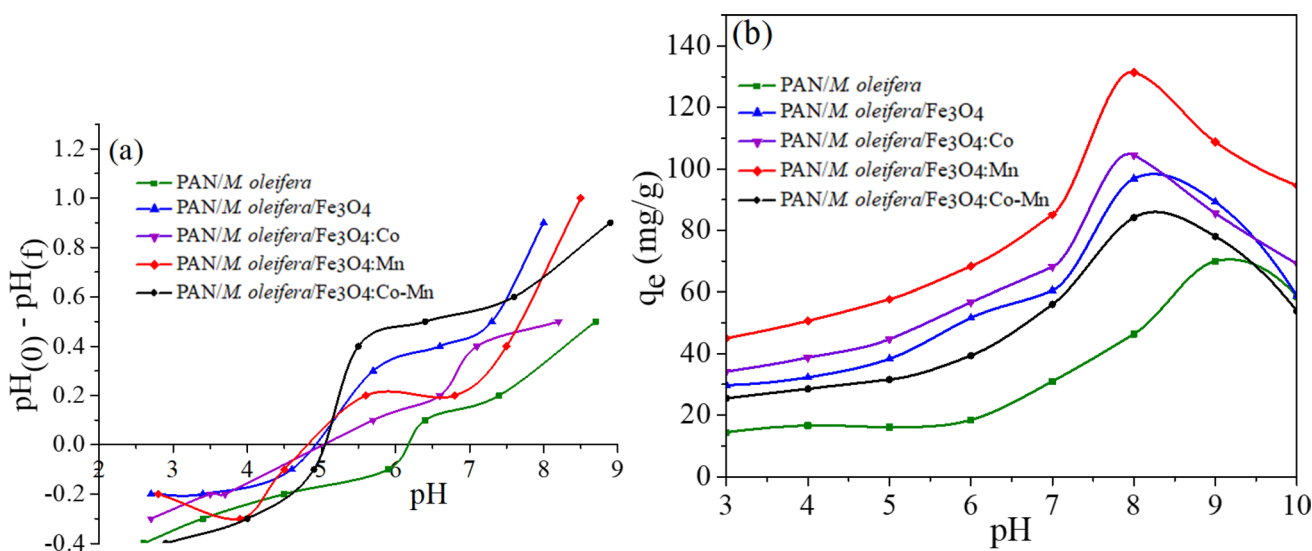
these planes in the patterns confirms the inverse-spinel structure of Fe$_3$O$_4$ (Warner et al. 2012).

The XRD patterns of metal-doped Fe$_3$O$_4$ were indexed and compared to the un-doped Fe$_3$O$_4$ (Fig. 4a). The 2theta peaks of the Co-doped Fe$_3$O$_4$ (Fig. 4b) showed peaks that were slightly shifted to higher angles due to slightly smaller atomic radius of Co^{2+}. The peak shifts are an indication of successful incorporation of Co^{2+} within the ferrite lattice structure. Figure 4c shows the Mn-doped Fe$_3$O$_4$ XDR pattern. There was no significant shifts observed compared to the free Fe$_3$O$_4$. Similar findings have been reported for Mn-doped Fe$_3$O$_4$ (Warner et al. 2012). The pattern also shows no peaks that correspond to MnO$_2$ or Mn$_3$O$_4$ further

Fig. 5 Plots of **a** pH$_{pzc}$ determination and **b** effect of pH on Pb(II) adsorption

indicate that the optimum adsorption capacity and removal efficiency occur at high pH (above pH_{PZC}) when the adsorbents surface become negatively charged. It stands to reason that the mechanism of adsorption is electrostatic attraction.

Effect of contact time

The influence of contact time on adsorption was examined between 30 and 150 min, while keeping the Pb(II) ion concentration at 5 mg/L, and at optimal solution pH of 8 (PAN/*M. oleifera*/MONPs) and 9 (PAN/*M. oleifera*). The results obtained are presented in Fig. 6. The figure shows that as the time is increased from 30 min, the adsorption capacity of the fiber mats increased until equilibrium was reached at 60 min (PAN/*M. oleifera*/MONPs) and 90 min (PAN/*M. oleifera*). A considerably faster adsorption with higher adsorption capacity was obtained by the fibers incorporated with MONPs, with the PAN/*M. oleifera*/Fe$_3$O$_4$:Mn fiber recording the highest adsorption capacity of 137.6 mg/g after 60 min. This was attributed to the high surface area of the MONPs as discussed previously.

Effect of initial Pb(II) concentration

The influence of initial Pb(II) ion concentration on the adsorption capacity and the removal efficiency of the fiber-matrix surface was studied between the range of 1–30 mg/L and under optimum pH and contact time of 60 min (PAN/*M. oleifera*/MONPs) and 90 min (PAN/*M. oleifera)*. Figure 7 shows that as initial concentration of Pb(II) ions increased, the adsorption capacity increased until saturation was approached at 20 mg/L. The increase in adsorption capacities of the fiber mats is due to the numbers of vacant active sites available for adsorption during the initial stage. As the
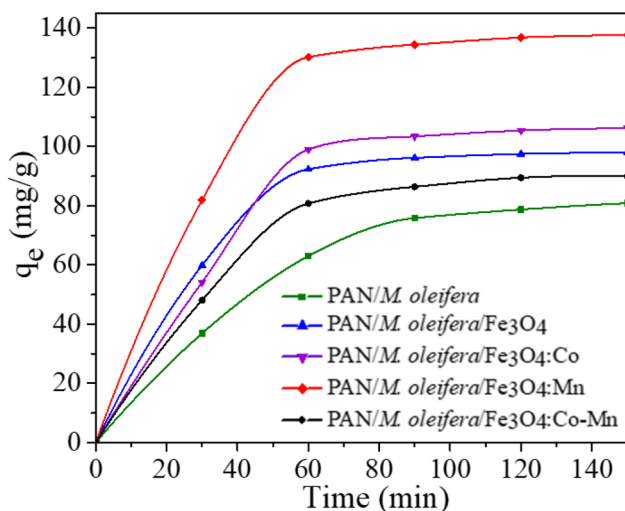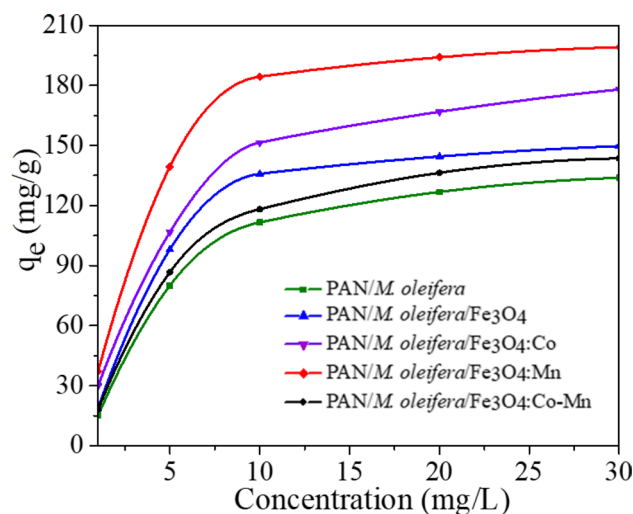

Fig. 7 Effect of initial Pb(II) concentration on Pb(II) adsorption

adsorption process proceeded, the remaining vacant surface sites decreased resulting in slowing down of the adsorption capacity until reaching the saturation point. The observed trends of the adsorption capacity in this study are in agreement with other previous reports on the adsorption of heavy metals by composite fibers (Lei et al. 2022; Tripathy et al. 2019). In order to further understand the adsorption behavior, the data obtained were fitted to the isotherm models.

Adsorption isotherms

The adsorption equilibria were best expressed using adsorption isotherm equations. The linear fitting plots of C_e/q_e versus C_e and log q_e versus log C_e for the Langmuir and Freundlich isotherm models, respectively, are shown in Fig. 8. The model parameters were determined and summarized in Table 2. From the graphs, the best isotherm fit was determined by the correlation coefficient (R^2). By comparing the R^2 values, the Langmuir model was determined to fit well with the linearized isotherm models. The Langmuir isotherm describes the adsorption sites as homogenously distributed on the adsorbents and the adsorption process is considered monolayer adsorption. It can be observed that q_m ranged from 172.4 to 227.3 mg/g with the PAN/*M. oleifera*/Fe$_3$O$_4$:Mn fiber recording the highest q_m value (227.3 mg/g). This indicates that the PAN/*M. oleifera*/Fe$_3$O$_4$:Mn fiber had the highest amount of Pb(II) ions adsorbed. The PAN/*M. oleifera*/Fe$_3$O$_4$:Mn fiber also recorded the highest K_L value of 0.272 L/mg implying a strong adsorption interaction.

The R_L values for the adsorbents were determined to range between 0.11 and 0.88. The R_L values specify if the adsorption is favorable ($0 < R_L < 1$), unfavorable ($R_L > 1$), irreversible ($R_L = 0$) or linear ($R_L = 1$). In this case, the fibers demonstrate a favorable Pb(II) adsorption process.
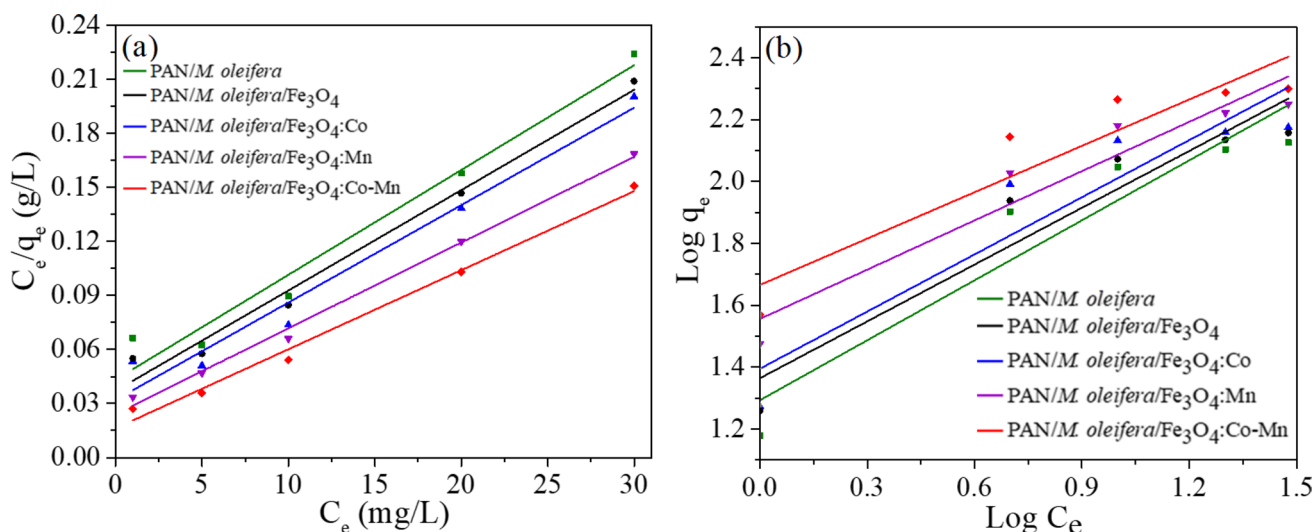

Fig. 6 Effect of contact time on Pb(II) adsorption

Fig. 8 The fitted lines of **a** the Langmuir and **b** Freundlich isotherms

Table 2 Fitting parameters of Langmuir and Freundlich isotherm models

Adsorbent	Langmuir model			Freundlich model		
	R^2	K_L (L/mg)	q_m (mg/g)	R^2	K_F (mg/g)	n
PAN/*M. oleifera*	0.97	0.134	172.4	0.90	23.43	1.557
PAN/*M. oleifera*/Fe$_3$O$_4$	0.98	0.169	185.2	0.87	24.84	1.626
PAN/*M. oleifera*/Fe$_3$O$_4$:Co	0.97	0.200	208.3	0.92	35.96	1.885
PAN/*M. oleifera*/Fe$_3$O$_4$:Mn	0.99	0.272	227.3	0.88	46.29	1.991
PAN/*M. oleifera*/Fe$_3$O$_4$:Co-Mn	0.98	0.151	178.6	0.90	23.12	1.633

Adsorption kinetics

In order to understand the adsorption kinetics of Pb(II) ions by the fibers, the pseudo-first-order and pseudo-second-order kinetic models were used to test the experimental data. The linear fitting plots of log (q_e-q_t) versus t and t/q_t versus t for the pseudo-first-order and pseudo-second-order models, respectively, are depicted in Fig. 9. According to R^2 values, the kinetic model that best fit the data was the pseudo-second-order model. The model is based on the assumption that chemisorption is the rate-determining step. Table 3 summarizes the calculated parameters from the fitted models.

Based on the pseudo-second-order model, it can be seen that q_e values ranged between 87.71 and 144.97 mg/g with the highest value obtained by the PAN/*M. oleifera*/Fe$_3$O$_4$:Mn fiber. This implies that the PAN/*M. oleifera*/Fe$_3$O$_4$:Mn fiber had the highest amount of Pb(II) ions adsorbed at equilibrium. Additionally, the experimentally determined values of q_e (Fig. 6) were very close to the calculated values in the pseudo-second-order model. This supports the applicability of the pseudo-second-order model.

A comparison of the maximum adsorption capacities with similar adsorbents is shown in Table 4. As observed, the fabricated PAN/*M. oleifera*/Fe$_3$O$_4$:Mn adsorbent performs better compared to other adsorbents for removing Pb(II) ions. This may be due to the porous nature of the adsorbent coupled with the presence of carboxyl and hydroxyl functional groups from the *M. oleifera* seed extract which can increase surface complexation with metal ions. The PAN/*M. oleifera*/Fe$_3$O$_4$:Mn composite mat can therefore be considered as a promising adsorbent for wastewater treatment due to its performance.

Conclusion

In this study, we demonstrated the fabrication of multicomposite fibers containing *M. oleifera* seed biomass, metal oxide nanoparticles and PAN using electrospinning. Their capability as adsorbents for Pb(II) ions in aqueous solution was successfully investigated using a batch adsorption process. Evaluation of the adsorption behavior of the PAN/*M. oleifera*/MONPs composite nanofibers for Pb(II) ions adsorption at optimal pH 8 and contact time 60 min revealed the adsorption followed the Langmuir isotherm and the pseudo-second-order kinetic model. The maximum
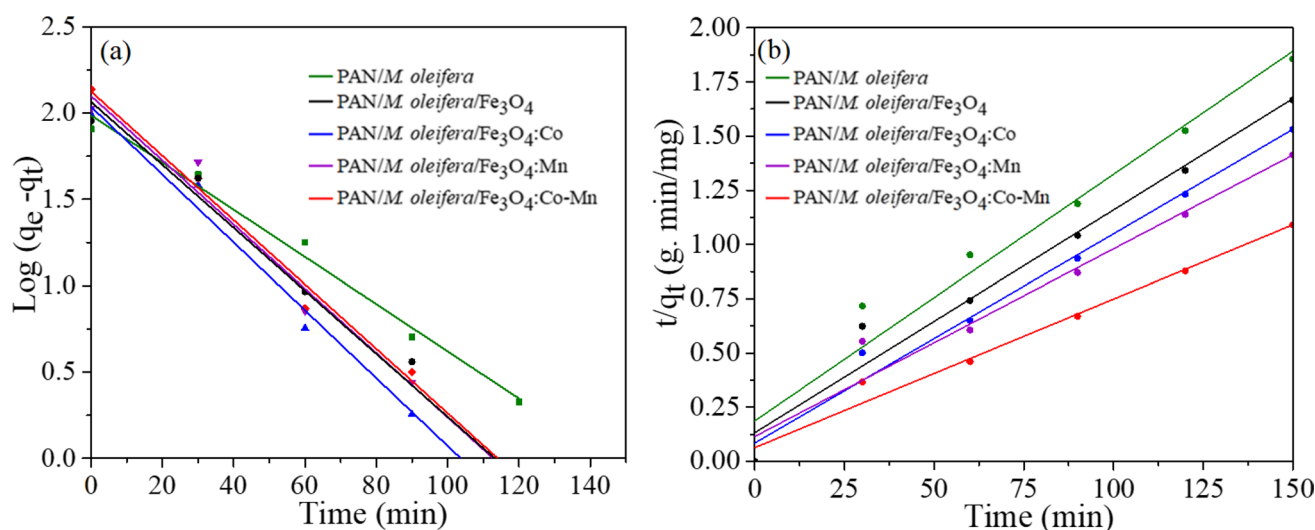
Fig. 9 The fitted lines of **a** pseudo-first-order and **b** pseudo-second-order models

Table 3 Fitting parameters of pseudo-first-order and pseudo-second-order models

Adsorbent	Pseudo-first-order model			Pseudo-second-order model		
	R^2	q_e (mg/g)	k_1 (h^{-1})	R^2	q_e (mg/g)	k_2 (g/g h)
PAN/*M. oleifera*	0.92	94.24	1.206	0.97	87.71	0.015
PAN/*M. oleifera*/Fe$_3$O$_4$	0.73	72.93	1.377	0.98	104.17	0.065
PAN/*M. oleifera*/Fe$_3$O$_4$:Co	0.93	92.56	1.494	0.96	114.94	0.040
PAN/*M. oleifera*/Fe$_3$O$_4$:Mn	0.94	100.05	1.366	0.98	144.97	0.045
PAN/*M. oleifera*/Fe$_3$O$_4$:Co-Mn	0.93	86.36	1.296	0.97	97.09	0.049

Table 4 Pb(II) ion maximum adsorption capacity of different adsorbents

Adsorbents	q_m (mg/g)	References
PVA/ Chitosan/Aminated-Fe$_3$O$_4$	21.2	Koushkbaghi et al. (2017
Polyaniline/CoFeC$_6$N$_6$	13.6	Moazezi et al. (2018
Polydopamine/PAN/MnO$_2$	185.2	Yanzi et al. (2018)
Cellulose nanofibrils/PVA/acrylic acid	131.5	Jiarong et al. (2018)
PAN/Hydrous MnO$_2$	194.4	Yadav et al. (2021)
Cellulose/Fe$_3$O$_4$	81.0	Vázquez-Guerrero et al. (2021)
PAN/*M. oleifera*/Fe$_3$O$_4$:Mn	227.3	This study

adsorption capacity ranged between 172.4 and 227.3 mg/g with the PAN/*M. oleifera*/Fe$_3$O$_4$:Mn fiber recording the highest value. The results demonstrate the effectiveness of incorporating cost effective, nontoxic and indigenous materials as potential adsorbents for Pb(II) ion removal from wastewater.

Declarations

Conflict of interest The authors declare that they have no known competing financial interests or personal relationships that could have appeared to influence the work reported in this paper.

References

Ali EN (2016) Removal of copper from water system using moringa oleifera press cake. Int Conf Agric Civ Environ Eng 16:15–18. https://doi.org/10.17758/URUAE.AE0416214

An J, Zhang H, Zhang J, Zhao Y, Yuan X (2009) Preparation and antibacterial activity of electrospun chitosan/poly (ethylene oxide) membranes containing silver nanoparticles. Colloid Polym Sci 287(12):1425–1434

Araújo CS, Alves VN, Rezende HC, Almeida IL, de Assunção RM, Tarley CR, Segatelli MG, Coelho NMM (2010) Characterization and use of *Moringa oleifera* seeds as biosorbent for removing metal ions from aqueous effluents. Water Sci Technol 62(9):2198–2203. https://doi.org/10.2166/wst.2010.419

Atacan K, Özacar M, Özacar M (2018) Investigation of antibacterial properties of novel papain immobilized on tannic acid modified Ag/CuFe$_2$O$_4$ magnetic nanoparticles. Int J Biol Macromol 109:720–731. https://doi.org/10.1016/j.ijbiomac.2017.12.066

Babel S, Kurniawan TA (2004) Cr (VI) removal from synthetic wastewater using coconut shell charcoal and commercial activated carbon modified with oxidizing agents and/or chitosan. Chemosphere 54(7):951–967. https://doi.org/10.1016/j.chemosphere.2003.10.001

Bahmani P, Maleki A, Daraei H, Rezaee R, Khamforoush M, Dehestani Athar S, Gharibi F, Ziaee AH, McKay G (2019) Application of modified electrospun nanofiber membranes with α-Fe$_2$O$_3$ nanoparticles in arsenate removal from aqueous media. Environ Sci Pollut Res 26:21993–22009

Bharathi KS, Ramesh ST (2013) Removal of dyes using agricultural waste as low-cost adsorbents: a review. Appl Water Sci 3(4):773–790. https://doi.org/10.1007/s13201-013-0117-y

Bhutada PR, Jadhav AJ, Pinjari DV, Nemade PR, Jain RD (2016) Solvent assisted extraction of oil from *Moringa oleifera* Lam Seeds. Ind Crops Prod 82:74–80. https://doi.org/10.1016/j.indcrop.2015.12.004

Cai J, Lei M, Zhang Q, He JR, Chen T, Liu S, Fu SH, Li TT, Liu G, Fei P (2017) Electrospun composite nanofiber mats of Cellulose@ Organically modified montmorillonite for heavy metal ion removal: Design, characterization, evaluation of absorption performance. Appl Sci Manuf 92:10–16. https://doi.org/10.1016/j.compositesa.2016.10.034

Chakrabarti S, Mandal SK, Chaudhuri S (2005) Cobalt doped γ-Fe$_2$O$_3$ nanoparticles: synthesis and magnetic properties. Nanotechnology 16(4):506

Chang J, Wang J, Qu J, Li YV, Ma L, Wang L, Wang X, Pan K (2016) Preparation of α-Fe$_2$O$_3$/polyacrylonitrile nanofiber mat as an effective lead adsorbent. Environ Sci Nano 3(4):894–901. https://doi.org/10.1039/C6EN00088F

Chen Y, Sui L, Fang H, Ding C, Li Z, Jiang S, Hou H (2019) Superior mechanical enhancement of epoxy composites reinforced by polyimide nanofibers via a vacuum-assisted hot-pressing. Compos Sci Technol 174:20–26. https://doi.org/10.1016/j.compscitech.2019.02.012

Crini G, Lichtfouse E, Wilson LD, Morin-Crini N (2018) Green adsorbents for pollutant removal. Environ Chem Sustain World 18:23–71

Cui J, Li F, Wang Y, Zhang Q, Ma W, Huang C (2020) Electrospun nanofiber membranes for wastewater treatment applications. Sep Purif Technol 250:117116. https://doi.org/10.1016/j.seppur.2020.117116

Dabrowski A, Hubicki Z, Podkoscielny P, Robens E (2004) Selective removal of the heavy metal ions from waters and industrial wastewaters by ion-exchange method. Chemosphere 56(2):91–106. https://doi.org/10.1016/j.chemosphere.2004.03.006

Deitzel JM, Kosik W, McKnight SH, Tan NB, DeSimone JM, Crette S (2002) Electrospinning of polymer nanofibers with specific surface chemistry. Polymer 43:1025–1029. https://doi.org/10.1016/S0032-3861(01)00594-8

Deliyanni EA, Bakoyannakis DN, Zouboulis AI, Matis KA (2003) Sorption of As (V) ions by akaganeite-type nanocrystals. Chemosphere 50(1):155–163

Deng Y, Lu T, Cui J, Samal SK, Xiong R, Huang C (2021) Bio-based electrospun nanofiber as building blocks for a novel eco-friendly air filtration membrane: a review. Sep Purif Technol 277:119623. https://doi.org/10.1016/j.seppur.2021.119623

Dos Santos TRT, Bongiovani MC, Silva MF, Nishi L, Coldebella PF, Vieira MF, Bergamasco R (2016) Trihalomethanes minimization in drinking water by coagulation/flocculation/sedimentation with natural coagulant *Moringa oleifera* Lam and activated carbon filtration. Can J Chem Eng 94(7):1277–1284. https://doi.org/10.1002/cjce.22506

Duan B, Yuan X, Zhu Y, Zhang Y, Li X, Zhang Y, Yao K (2006) A nanofibrous composite membrane of PLGA–chitosan/PVA prepared by electrospinning. Eur Polym J 42(9):2013–2022. https://doi.org/10.1016/j.eurpolymj.2006.04.021

Fan L, Luo C, Sun M, Qiu H (2012) Synthesis of graphene oxide decorated with magnetic cyclodextrin for fast chromium removal. J Mater Chem 22:24577–24583. https://doi.org/10.1039/C2JM35378D

Fayemi OE, Ekennia AC, Katata-Seru L, Ebokaiwe AP, Ijomone OM, Onwudiwe DC, Ebenso EE (2018) Antimicrobial and wound healing properties of polyacrylonitrile-moringa extract nanofibers. ACS Omega 3(5):4791–4797

Fu F, Wang Q (2011) Removal of heavy metal ions from wastewaters: a review. J Environ Manag 92(3):407–418. https://doi.org/10.1016/j.jenvman.2010.11.011

Galiano F, Briceño K, Marino T, Molino A, Christensen KV, Figoli A (2018) Advances in biopolymer-based membrane preparation and applications. J Membr Sci 564:562–586. https://doi.org/10.1016/j.memsci.2018.07.059

Ghiloufi I, El-Ghoul J, Modwi A, El-Mir L (2016) Preparation and characterization of Ca-doped zinc oxide nanoparticles for heavy metal removal from aqueous solution. MRS Adv 1(53):3607–3612. https://doi.org/10.1557/adv.2016.511

Ghomi AG, Asasian-Kolur N, Sharifian S, Golnaraghi A (2020) Biosorpion for sustainable recovery of precious metals from wastewater. J Environ Chem Eng 8(4):103996. https://doi.org/10.1016/j.jece.2020.103996

Guo C, Hu Y, Qian H, Ning J, Xu S (2011) Magnetite (Fe$_3$O$_4$) tetrakaidecahedral microcrystals: synthesis, characterization,

and micro-Raman study. Mater Charact 62(1):148–151. https://doi.org/10.1016/j.matchar.2010.10.016

Hasan HA, Abdullah SR, Kofli NT, Kamarudin SK (2012) Isotherm equilibria of Mn^{2+} biosorption in drinking water treatment by locally isolated Bacillus species and sewage activated sludge. J Environ Manag 111:34–43. https://doi.org/10.1016/j.jenvman.2012.06.027

Ibrahim AO, Adegoke AK, Adegoke RO, AbdulWahab YA, Oyelami VB, Adesina MO (2021) Adsorptive removal of different pollutants using metal-organic framework adsorbents. J Mol Liq 333:115593. https://doi.org/10.1016/j.molliq.2021.115593

Ibrahim NA, Bibi S, Khan AK, Murtaza G (2022) Development and butyrylcholinesterase/monoamine oxidase inhibition potential of PVA-Moringa oleifera developed nanofibers. J Exp Nanosci 17(1):34–46. https://doi.org/10.1080/17458080.2021.2016712

Ignatova M, Manolova N, Rashkov I (2007) Novel antibacterial fibers of quaternized chitosan and poly (vinyl pyrrolidone) prepared by electrospinning. Eur Polym J 43(4):1112–1122. https://doi.org/10.1016/j.eurpolymj.2007.01.012

Jain R, Shetty S, Yadav KS (2020) Unfolding the electrospinning potential of biopolymers for preparation of nanofibers. J Drug Deliv Sci Technol 57:101604. https://doi.org/10.1016/j.jddst.2020.101604

Jiarong S, Cuihua T, Yiqiang W, Xianjun L, Sha L, Yan Q, Zheng J (2018) Cellulose nanofibrils aerogel cross-linked by poly (vinyl alcohol) and acrylic acid for efficient and recycled adsorption with heavy metal ions. J Nanosci Nanotechnol 18:4167–4175. https://doi.org/10.1166/jnn.2018.15264

Jung KH, Huh MW, Meng W, Yuan J, Hyun SH, Bae JS, Hudson SM, Kang IK (2007) Preparation and antibacterial activity of PET/chitosan nanofibrous mats using an electrospinning technique. J Appl Polym Sci 105(5):2816–2823. https://doi.org/10.1002/app.25594

Keshtkar AR, Tabatabaeefar A, Vaneghi AS, Moosavian MA (2016) Electrospun polyvinylpyrrolidone/silica/3-aminopropyltriethoxysilane composite nanofiber adsorbent: preparation, characterization and its application for heavy metal ions removal from aqueous solution. J Environ Chem Eng 4(1):1248–1258. https://doi.org/10.1016/j.jece.2016.01.023

Khademian E, Salehi E, Sanaeepur H, Galiano H, Figoli A (2020) A systematic review on carbohydrate biopolymers for adsorptive remediation of copper ions from aqueous environments-part A: Classification and modification strategies. Sci Total Environ 738:139829. https://doi.org/10.1016/j.scitotenv.2020.139829

Khalid N, Aqeel M, Noman A, Khan SM, Akhter N (2021) Interactions and effects of microplastics with heavy metals in aquatic and terrestrial environments. Environ Pollut 290:118104. https://doi.org/10.1016/j.envpol.2021.118104

Khlifi R, Hamza-Chaffai A (2010) Head and neck cancer due to heavy metal exposure via tobacco smoking and professional exposure: a review. Toxicol Appl Pharmacol 248(2):71–88. https://doi.org/10.1016/j.taap.2010.08.003

Klencsár Z, Ábrahám A, Szabó L, Szabó EG, Stichleutner S, Kuzmann E, Homonnay Z, Tolnai G (2019) The effect of preparation conditions on magnetite nanoparticles obtained via chemical co-precipitation. Mater Chem Phys 223:122–132. https://doi.org/10.1016/j.matchemphys.2018.10.049

Koushkbaghi S, Zakialamdari A, Pishnamazi M, Ramandi HF, Aliabadi M, Irani M (2017) Aminated-Fe_3O_4 nanoparticles filled chitosan/PVA/PES dual layers nanofibrous membrane for the removal of Cr(VI) and Pb(II) ions from aqueous solutions in adsorption and membrane processes. Chem Eng J 337:169–182. https://doi.org/10.1016/j.cej.2017.12.075

Kumar KY, Muralidhara HB, Nayaka YA, Balasubramanyam J, Hanumanthappa H (2013) Low-cost synthesis of metal oxide nanoparticles and their application in adsorption of commercial dye and heavy metal ion in aqueous solution. Powder Technol 246:125–136. https://doi.org/10.1016/j.powtec.2013.05.017

Kyzas GZ, Kostoglou M, Lazaridis NK (2009) Copper and chromium (VI) removal by chitosan derivatives—equilibrium and kinetic studies. J Chem Eng 152:440–448. https://doi.org/10.1016/j.cej.2009.05.005

Lee J, Yoon J, Kim JH, Lee T, Byun H (2018) Electrospun PAN–GO composite nanofibers as water purification membranes. J Appl Polym Sci 35(7):45858. https://doi.org/10.1002/app.45858

Lei X, Wang Z, Qi J, Wang X, Chen Y, Li B, Zhou Y (2022) Preparation of Iron Carbon Composite Material by Extracting Iron from Bauxite Residue and Its Adsorption of Heavy Metal Cd(II). Bull Environ Contam Toxicol. https://doi.org/10.1007/s00128-022-03539-x

Li YH, Ding J, Luan Z, Di Z, Zhu Y, Xu C, Wu D, Wei B (2003) Competitive adsorption of Pb^{2+}, Cu^{2+} and Cd^{2+} ions from aqueous solutions by multiwalled carbon nanotubes. Carbon 41(14):2787–2792. https://doi.org/10.1016/S0008-6223(03)00392-0

Li Y, Zhao R, Chao S, Sun B, Wang C, Li X (2018a) Polydopamine coating assisted synthesis of MnO_2 loaded inorganic/organic composite electrospun fiber adsorbent for efficient removal of Pb^{2+} from water. Chem Eng J 344:277–289. https://doi.org/10.1016/j.cej.2018.03.044

Liu Q, Zhong LB, Zhao QB, Frear C, Zheng YM (2015) Synthesis of Fe_3O_4/polyacrylonitrile composite electrospun nanofiber mat for effective adsorption of tetracycline. ACS Appl Mater Interfaces 7(27):14573–14583. https://doi.org/10.1021/acsami.5b04598

Liu S, Huang J, Zhang W, Shi L, Yi K, Yu H, Zhang C, Li S, Li J (2022) Microplastics as a vehicle of heavy metals in aquatic environments: a review of adsorption factors mechanisms and biological effects. J Environ Manage 302:113995. https://doi.org/10.1016/j.jenvman.2021.113995

Martín DM, Faccini M, García MA, Amantia D (2018) Highly efficient removal of heavy metal ions from polluted water using ion-selective polyacrylonitrile nanofibers. J Environ Chem Eng 6(1):236–245. https://doi.org/10.1016/j.jece.2017.11.073

Mascolo MC, Pei Y, Ring TA (2013) Room temperature co-precipitation synthesis of magnetite nanoparticles in a large pH window with different bases. Mater 6(12):5549–5567

Mbakaan C, Ahemen I, Dejene FB, Onojah AD, Motloung SJ, Ocaya R, Reyes-Rojas A (2021) Structural and optical properties of nano-SiO_2 derived from the husk of some rice varieties and the effect of doping with Sm^{3+} ions. Opt Mater Express 11(4):965–987. https://doi.org/10.1364/OME.419552

Moazezi N, Baghdadi M, Hickner MA, Moosavian MA (2018) Modeling and experimental evaluation of Ni (II) and Pb (II) sorption from aqueous solutions using a polyaniline/$CoFeC_6N_6$ nanocomposite. J Chem Eng Data 63:741–750. https://doi.org/10.1021/acs.jced.7b00897

Montoya P, Marin T, Mejia S, Arnache O, Calderon JA (2017) Elucidation of the mechanism of electrochemical formation of magnetite nanoparticles by in situ raman spectroscopy. J Electrochem Soc 164(14):1056

Moonga G, Chisola MN, Berger U, Nowak D, Yabe J, Nakata H, Nakayama S, Ishizuka M, Bose-O'Reilly S (2022) Geospatial approach to investigate spatial clustering and hotspots of blood lead levels in children within Kabwe. Zambia Environ Res 207:112646. https://doi.org/10.1016/j.envres.2021.112646

Morillo MD, Magdi AM, Rodríguez M, García MA, Faccini M (2017) Aminated polyethylene terephthalate (PET) nanofibers for the selective removal of Pb(II) from polluted water. Mater 10(12):1352. https://doi.org/10.3390/ma10121352

Naiya TK, Bhattacharya AK, Das SK (2009) Adsorption of Cd (II) and Pb (II) from aqueous solutions on activated alumina. J Colloid Interface Sci 333(1):14–26. https://doi.org/10.1016/j.jcis.2009.01.003

Narayan M, Sadasivam R, Packirisamy G, Pichiah S (2022) Electrospun polyacrylonitrile-Moringa Olifera based nanofibrous bio-sorbent for remediation of Congo red dye. J Environ Manag 317:115294. https://doi.org/10.1016/j.jenvman.2022.115294

Ndabigengesere A, Narasiah KS (1998) Use of Moringa oleifera seeds as a primary coagulant in wastewater treatment. Environ Technol 19(8):789–800. https://doi.org/10.1080/09593331908616735

Nunes JS, De Vasconcelos CL, Cabral FAO, de Araújo JH, Pereira MR, Fonseca JLC (2006) Synthesis and characterization of poly (ethyl methacrylate-co-methacrylic acid) magnetic particles via miniemulsion polymerization. Polymer 47(22):7646–7652. https://doi.org/10.1016/j.polymer.2006.09.006

Nurlilasari P, Widiyastuti W, Setyawan H, Faizal F, Wada M, Lenggoro IW (2019) High-throughput production of magnetite nanoparticles prepared by the monopolar arrangement of iron electrodes in water. Chem Eng Sci 201:112–120. https://doi.org/10.1016/j.ces.2019.02.027

Okuda T, Baes AU, Nishijima W, Okada M (2001) Isolation and characterization of coagulant extracted from *Moringa oleifera* seed by salt solution. Water Res 35(2):405–410

Parlayıcı Ş, Yar A, Avcı A, Pehlivan E (2016) Removal of hexavalent chromium using polyacrylonitrile/titanium dioxide nanofiber membrane. Desalin Water Treat 57(34):16177–16183. https://doi.org/10.1080/19443994.2015.1077349

Pereao OK, Bode-Aluko C, Ndayambaje G, Fatoba O, Petrik LF (2017) Electrospinning: polymer nanofibre adsorbent applications for metal ion removal. J Polym Environ 25(4):1175–1189. https://doi.org/10.1007/s10924-016-0896-y

Ramakrishna S, Fujihara K, Teo WE, Yong T, Ma Z, Ramaseshan R (2006) Electrospun nanofibers: solving global issues. Mater Today 9(3):40–50. https://doi.org/10.1016/S1369-7021(06)71389-X

Raza ZA, Munim SA, Ayub A (2021) Recent developments in polysaccharide-based electrospun nanofibers for environmental applications. Carbohydr Res 510:108443. https://doi.org/10.1016/j.carres.2021.108443

Razzaz A, Ghorban S, Hosayni L, Irani M, Aliabadi M (2016) Chitosan nanofibers functionalized by TiO_2 nanoparticles for the removal of heavy metal ions. J Taiwan Inst Chem Eng 58:333–343. https://doi.org/10.1016/j.jtice.2015.06.003

Sakib MN, Mallik AK, Rahman MN (2021) Update on chitosan-based electrospun nanofibers for wastewater treatment: a review. Carbohydr Polym Technol Appl 2:100064. https://doi.org/10.1016/j.carpta.2021.100064

Sarkar S, Guibal E, Quignard F, SenGupta AK (2012) Polymer-supported metals and metal oxide nanoparticles: synthesis, characterization, and applications. J Nanoparticle Res 14(2):1–24

Sarode S, Upadhyay P, Khosa MA, Mak T, Shakir A, Song S, Ullah A (2019) Overview of wastewater treatment methods with special focus on biopolymer chitin-chitosan. Int J Biol Macromol 121:1086–1100. https://doi.org/10.1016/j.ijbiomac.2018.10.089

Suresh R, Prabu R, Vijayaraj A, Giribabu K, Stephen A, Narayanan V (2012) Facile synthesis of cobalt doped hematite nanospheres: magnetic and their electrochemical sensing properties. Mater Chem Phys 134:590–596. https://doi.org/10.1016/j.matchemphys.2012.03.034

Tan P, Wen J, Hu Y, Tan X (2016) Adsorption of Cu^{2+} and Cd^{2+} from aqueous solution by novel electrospun poly (vinyl alcohol)/graphene oxide nanofibers. RSC Adv 6(83):79641–79650. https://doi.org/10.1039/C6RA18052C

Tempelman K, Casanova S, Benes NE (2019) The effect of hydrocarbon pollution on polysulfone-based membranes in aqueous separations. Sep Purif Technol 224:348–355. https://doi.org/10.1016/j.seppur.2019.05.013

Tripathy M, Hota G (2019) Maghemite and graphene oxide embedded polyacrylonitrile electrospun nanofiber matrix for remediation of arsenate ions. ACS Appl Polym Mater 2(2):604–617. https://doi.org/10.1021/acsapm.9b00982

Vázquez-Guerrero A, Cortés-Martínez R, Alfaro-Cuevas-Villanueva R, Rivera-Muñoz EM, Huirache-Acuña R (2021) Cd (II) and Pb (II) adsorption using a composite obtained from moringa oleifera lam: cellulose nanofibrils impregnated with iron nanoparticles. Water 13(1):89. https://doi.org/10.3390/w13010089

Wahab A, Imran M, Ikram M, Naz M, Aqeel M, Rafiq A, Majeed H, Ali S (2019) Dye degradation property of cobalt and manganese doped iron oxide nanoparticles. Appl Nanosci 9(8):1823–1832. https://doi.org/10.1016/S0043-1354(00)00290-6

Wang H, Zhang P, Ma X, Jiang S, Huang Y, Zhai L, Jiang S (2014) Preparation, characterization of electrospun meso-hydroxylapatite nanofibers and their sorptions on Co(II). J Hazard Mater 265:158–165. https://doi.org/10.1016/j.jhazmat.2013.12.002

Warner CL, Chouyyok W, Mackie KE, Neiner D, Saraf LV, Droubay TC, Warner MG, Addleman RS (2012) Manganese doping of magnetic iron oxide nanoparticles: tailoring surface reactivity for a regenerable heavy metal sorbent. Langmuir 28(8):3931–3937. https://doi.org/10.1021/la2042235

Wen P, Wen Y, Zong MH, Linhardt RJ, Wu H (2017) Encapsulation of bioactive compound in electrospun fibers and its potential application. J Agric Food Chem 65(42):9161–9179. https://doi.org/10.1021/acs.jafc.7b02956

Wongkanya R, Chuysinuan P, Pengsuk C, Techasakul S, Lirdprapamongkol K, Svasti J, Nooeaid P (2017) Electrospinning of alginate/soy protein isolated nanofibers and their release characteristics for biomedical applications. J Sci Adv Mater Dev 2(3):309–316. https://doi.org/10.1016/j.jsamd.2017.05.010

Xu J, Zhang J, Gao W, Liang H, Wang H, Li J (2009) Preparation of chitosan/PLA blend micro/nanofibers by electrospinning. Mater Lett 63(8):658–660. https://doi.org/10.1016/j.matlet.2008.12.014

Yadav P, Farnood R, Kumar V (2021) HMO-incorporated electrospun nanofiber recyclable membranes: Characterization and adsorptive performance for Pb(II) and As(V). J Environ Chem Eng 9:2213–3437. https://doi.org/10.1016/j.jece.2021.106507

Yong Y, Hua W, Jianhang H (2021) Co-treatment of electroplating sludge, copper slag, and spent cathode carbon for recovering and solidifying heavy metals. J Hazard Mater 417:126020. https://doi.org/10.1016/j.jhazmat.2021.126020

Zhao R, Li X, Sun S, Shen M, Tan X, Ding Y, Jiang Z, Wang C (2015) Preparation of phosphorylated polyacrylonitrile-based nanofiber mat and its application for heavy metal ion removal. Chem Eng J 268:290–299. https://doi.org/10.1016/j.cej.2015.01.061

Zheng M, Sun Z, Han H, Zhang Z, Ma W, Xu C (2021) Enhanced coagulation coupled with heavy metal capturing for heavy metals removal from coal gasification brine and a novel mathematical model. J Water Process Eng 40:101954. https://doi.org/10.1016/j.jwpe.2021.101954